JPE 9-3-17

ICPE'07 Selected Paper

SVPWM Overmodulation Scheme of Three-Level Inverters for Vector Controlled Induction Motor Drives

Kyoung-Min Kwon*, Jae-Moon Lee**, Jin-Mok Lee*, and Jaeho Choi†

†* School of Electrical and Computer Engineering, Chungbuk National University, Cheongju, Korea
** R&D Center, LS Industrial Systems Co. Ltd., Cheonan, Korea

ABSTRACT

This paper describes a SVPWM overmodulation scheme of NPC type three-level inverter for traction drives which extends the modulation index from MI=0.907 to unity . SVPWM strategy is organized by two operation modes of under-modulation and over-modulation. The switching states under the under-modulation modes are determined by dividing them with two linear regions and one hybrid region the same as the conventional three-level inverter. On the other hand, under the over-modulation mode, they are generated by doing it with two over-modulation regions the same as the conventional over-modulation strategy of a two level inverter. Following the description of over-modulation scheme of a three-level inverter, the system description of a vector controlled induction motor for traction drives has been discussed. Finally, the validity of the proposed modulation algorithm has been verified through simulation and experimental results.

Keywords: Overmodulation, SVPWM, NPC type three-level inverter, Indirect vector control

1. Introduction

This paper presents an overmodulation scheme of NPC type three-level inverter and an indirect vector control of induction motor for traction drives. Recently railway vehicles have operated at higher speeds within the limited plant for higher efficiency. The conventional railway vehicle has used the vector control to the modulation factor of 90.7% with space vector PWM (SVPWM) and used the slip-frequency control to six-step mode. The slip-frequency control is suitable for traction drives, because the drive patterns of electric railway systems do not request a rapid change. However, that control can not realize a quick torque response. In high-speed trains, the slip between train wheels and rails is likely to occur, and the fast torque control is crucial to overcome this slip problem. The vector control provides an instantaneous torque response because it is possible to control the flux and torque of the induction motor independently. An overmodulation scheme of SVPWM with modulation factor 90.7% to unity is essential if the drive can meet the operation at extended speed including the field weakening region in vector control with higher torque and power characteristics. The overmodulation strategy of a two-level inverter and its implementation has been studied [1,2].

The NPC type three-level inverter has three output voltage levels. With this circuit configuration, the voltage stress on its power switching devices is half that of the

Manuscript received January 30, 2009; revised April 8, 2009
†Corresponding Author: choi@chungbuk.ac.kr
Tel: +82-43-261-2425, Fax: +82-43-276-7217, Chungbuk Nat'l Univ.
*School of Electrical and Computer Engineering, Chungbuk National University, Cheongju, Korea
**R&D Center, LS Industrial Systems Co. Ltd., Cheonan, Korea

conventional two-level inverter. Because of this nature, it has been applied to the medium and high voltage drives. In addition to the capability to handle the high voltage, the NPC type three-level inverter has favorable features; lower line to line and common-mode voltage steps, more frequent voltage steps in one carrier cycle, and lower ripple components in the output current at the same carrier frequency. These features lead to significant advantages for motor drives over the conventional two-level inverters in the form of lower stresses to the motor windings and bearings, less influence of noise to the adjacent equipment, etc [3]. Recently, most Japanese electrical train companies have developed a three-level PWM inverter drive system for traction drives. It is well known that the three-level configuration has greatly reduced the size of the main transformer and traction-motor, the current harmonics in the signaling band, the acoustic noise, and the volume and weight of the equipment [4]-[7]. Also, the power rating of the system can be increased. However, SVPWM of a three-level inverter is considerably more complex than that of a two-level inverter due to the large number of inverter switching states. Besides, there is the problem of neutral point voltage balancing [8]. There have been some studies on the over-modulation strategy of three-level inverters, but few of them are focused on the application of traction drives. Most of them are limited to the modulation itself and lack of experimental implementation [9]-[11].

This paper describes a SVPWM over-modulation scheme of the NPC type three-level inverter that extends the modulation index from MI=0.907 to unity [12]. SVPWM strategy is organized by two operation modes of under-modulation and over-modulation. The switching states under the under-modulation mode are determined by dividing them with two linear regions and one hybrid region the same as the conventional three-level inverter. On the other hand, under the over-modulation mode, they are generated by doing this with two over-modulation regions which is the same as the conventional over-modulation strategy of the two level inverter. Following the description of the over-modulation scheme of the three-level inverter, the system description of a vector controlled induction motor for traction drives has been discussed. Finally, the validity of the proposed modulation algorithm has been verified through the simulation and experimental results.

2. NPC type Three-level Inverter

The NPC type three-level inverter has three output voltage levels. With this circuit configuration, the voltage stress on its power switching devices is half that of the conventional two-level inverter. Because of this nature, it has been applied to the medium and high voltage drives. In addition to the capability to handle the high voltage, the NPC type three-level inverter has favorable features; lower line to line and common-mode voltage steps, more frequent voltage steps in one carrier cycle, and lower ripple components in the output current at the same carrier frequency. These features lead to significant advantages for motor drives over the conventional two-level inverters in the form of lower stresses to the motor windings and bearings, less influence of noise to the adjacent equipment, etc.

Fig. 1 shows the schematic diagram of a three-level IGBT inverter with induction motor load. For power conversion, a similar unit is connected at the DC input in an inverse manner.

The phase U, for example, gets the state P when the switches U1 and U2 are on, whereas it gets the state N when the switches U3 and U4 are on. At neutral-point clamping, the phase gets the O state when either U2 or U3 conducts depending on positive or negative phase current polarity, respectively. The switching states of the three-level inverter can be summarized as shown in Table 1, where U, V, and W are the phases and P, N, and O are dc-bus points.

The total switching states consist of 27 and can be

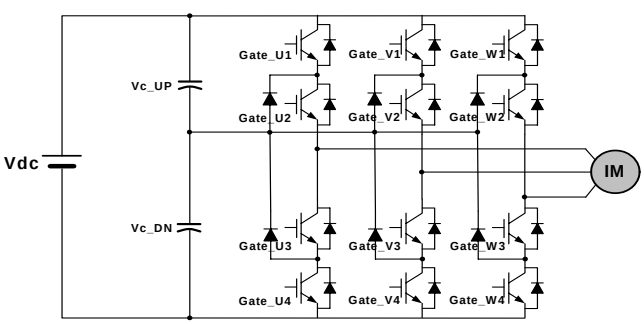

Fig. 1. Schematic diagram of three-level inverter with induction motor load.

described as shown in Fig. 2. The corresponding 27 switching states of the three-level inverter indicating each state with the combination of P, N, and O states are classified by four voltage vectors according to the magnitude value of voltage vector. The four voltage vectors are separated by zero vector (ZV), small vector (SV), middle vector (MV), and large vector (LV). These four voltage vectors are summarized in Table 2. Evidently, neutral current will flow through the point O in all the states except the zero states and the outer hexagon has six large sector(A-F) as shown and each large sector has four small sector(1-4), giving altogether 24 regions of operation.

An overmodulation strategy for higher voltage utilization is driven from the developing Fourier series expansion of the reference phase voltage waveform which generates the desired fundamental component. According to the modulation index (MI), the PWM control range can be divided into three regions as one linear region $(0 \le MI \le 0.907)$ of undermodulation mode and two overmodulation modes of overmodulation region I $(0.907 \le MI \le 0.952)$ and overmodulation region II $(0.952 \le MI \le 1)$ as shown in Fig. 3.

Table 1 Switching states of three-level inverter

Switching State	Gate-(X) X=[U, V, W]				$V_{(X)O}$ [Node voltage]
	X-1	X-2	X-3	X-4	
P	ON	ON	OFF	OFF	$+V_{dc}/2$
O	OFF	ON	ON	OFF	0
N	OFF	OFF	ON	ON	$-V_{dc}/2$

Table 2 Voltage vectors according to switching states

Switching vector		Switching state (U V W)			Capacitor state V_{C_UP}	Capacitor state V_{C_DN}	voltage vector
ZV		(PPP)	(OOO)	(NNN)	0	0	0
SV	USV	(POO)	(PPO)	(OPO)	−	+	$\frac{V_{dc}}{3}$
		(OPP)	(OOP)	(POP)			
	LSV	(ONN)	(OON)	(NON)	+	−	
		(NOO)	(NNO)	(ONO)			
MV		(PON)	(OPN)	(NPO)	+/−	+/−	$\frac{V_{dc}}{\sqrt{3}}$
		(NOP)	(ONP)	(PNO)			
LV		(PNN)	(PPN)	(NPN)	+/−	+/−	$\frac{2V_{dc}}{3}$
		(NPP)	(NNP)	(PNP)			

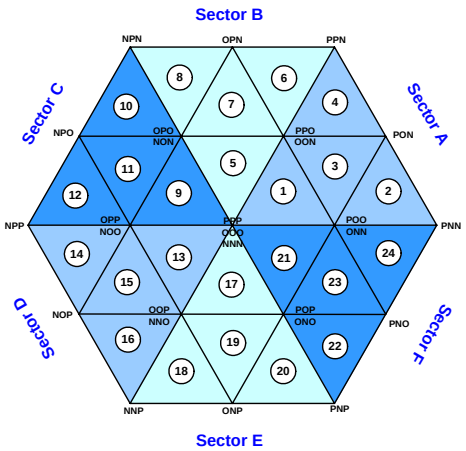

Fig. 2. Space voltage vector diagram of NPC type three-level Inverter.

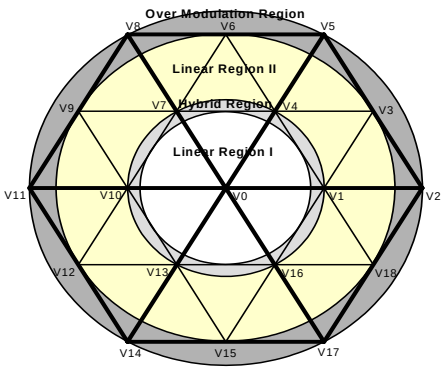

Fig. 3. Operation region of three-level inverter for overmodulated PWM.

2.1 Undermodulation mode $(0 \le MI \le 0.907)$

The linear region is located in the inscribed circle of an outer hexagon. It consists of linear region mode I $(0 \le MI \le 0.433)$, linear region II $(0.5 \le MI \le 0.907)$, and their interfaced hybrid region $(0.433 \le MI \le 0.5)$. Linear region mode I is located in the inscribed circle of inner hexagon.

The Hybrid region is located between the inscribed circle of inner hexagon and the circumscribed circle of the inner hexagon. Linear region mode II is located between the circumscribed circle of inner hexagon and the inscribed circle of outer hexagon. Linear region mode I has 3 steps output line-to-line voltage like as 2-level inverter. Linear region mode II has 5 steps output line-to-line voltage. And hybrid region has the characteristics of linear region mode I and linear region mode II.

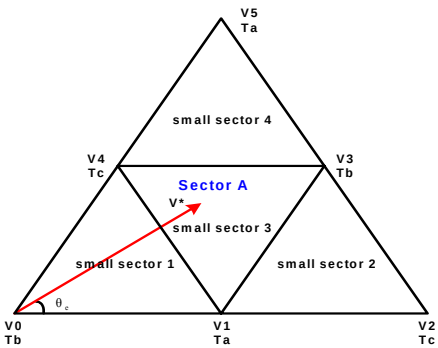

Fig. 4. Voltage vector in large sector A.

Table 3 Duration time of voltage vectors in each small sector

small sector	T_a	T_b	T_c
1	$2kT_s \sin(\frac{\pi}{3}-\theta_e)$	$T_s[1-2k\sin(\theta_e+\frac{\pi}{3})]$	$2kT_s \sin\theta_e$
2	$2T_s[1-k\sin(\theta_e+\frac{\pi}{3})]$	$2kT_s \sin\theta_e$	$T_s[2k\sin(\frac{\pi}{3}-\theta_e)-1]$
3	$T_s[1-2k\sin\theta_e]$	$T_s[2k\sin(\theta_e+\frac{\pi}{3})-1]$	$T_s[2k\sin(\theta_e-\frac{\pi}{3})+1]$
4	$T_s[2k\sin\theta_e-1]$	$2kT_s \sin(\frac{\pi}{3}-\theta_e)$	$2T_s[1-k\sin(\theta_e+\frac{\pi}{3})]$

T_s : sampling time for reference vector

$k=\sqrt{3}V^*/Vdc=(2\sqrt{3}/\pi)\cdot MI$: modulation amplitude ratio

Figure 4 shows one of six large sectors in the linear region. Each large triangle can be divided into four small sectors 1, 2, 3, and 4. In SVPWM method, the inverter voltage vectors corresponding to the apexes of the triangle which includes the voltage reference vector are generally selected to minimize the harmonic components of the output line-to-line voltage.

Table 3 shows the analytical time expression for all the small sectors in the large sector A. These time intervals can be applied to the other large sectors by a phase shift of the voltage reference vector. These time intervals are distributed appropriately so as to generate the symmetrical PWM pulses with a neutral-point voltage balancing. Note that the sequence in opposite sectors (A-D, B-E and C-F) is selected to be of a complimentary nature for the voltage balancing of a neutral-point.

2.2 Overmodulation mode $(0.907 \le MI \le 1)$

1) Over-modulation region I $(0.907 \le MI \le 0.952)$

In the over-modulation region I, the voltage reference vector V^* exceeds the outer hexagon which is the boundary of making a maximum voltage value. So V^* is boosted up to V_c^* for the compensation of voltage loss due to the excess region. Figure 5 presents the trajectory of V^*, V_c^*, and V_r^* which is the actual reference vector applying to control in the time domain. The angle α_r is the reference angle which is an intersection of V_c^* and boundary of the hexagon. The regions of V_r^* present four kinds of equations per π/2 for the angle of the voltage reference vector, as shown in (1) to (4). In both side regions of each triangle sector to α_r, V_c^* is used to compensate the voltage loss due to the excess of the outer hexagon. Plus it generates the maximum voltage value to follow the outer hexagon between those two regions. The value of taking the fundamental component of V_r^* is directly proportional to MI. V_r^* is presented in Fig. 3.

$$f_1 = \frac{V_{dc}}{\sqrt{3}}\tan\theta, \qquad 0 \le \theta \le \left(\frac{\pi}{6}-\alpha_r\right) \tag{1}$$

$$f_2 = \frac{V_{dc}}{\sqrt{3}\cos\left(\frac{\pi}{6}-\alpha_r\right)}\sin\theta, \qquad \left(\frac{\pi}{6}-\alpha_r\right) \le \theta \le \left(\frac{\pi}{6}+\alpha_r\right) \tag{2}$$

$$f_3 = \frac{V_{dc}}{\sqrt{3}\cos\left(\frac{\pi}{3}-\theta\right)}\sin\theta, \qquad \left(\frac{\pi}{6}+\alpha_r\right) \le \theta \le \left(\frac{\pi}{2}-\alpha_r\right) \tag{3}$$

$$f_4 = \frac{V_{dc}}{\sqrt{3}\cos\left(\frac{\pi}{6}-\alpha_r\right)}\sin\theta, \qquad \left(\frac{\pi}{2}-\alpha_r\right) \le \theta \le \frac{\pi}{2} \tag{4}$$

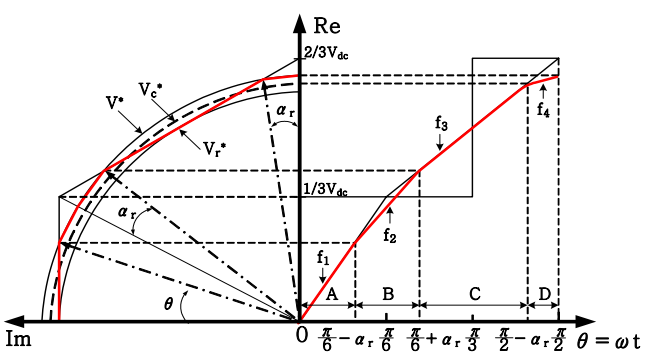

Fig. 5. Trajectory of reference voltage vector and phase voltage waveform in over-modulation region I.

where $\theta = \omega_e t$ and ω_e is an angular velocity of the voltage reference vector.

Expanding from (1) to (4) in the Fourier series and taking its fundamental component, the resultant equation can be expressed as

$$F(\alpha_r) = \frac{4}{\pi}\left[\int_A f_1 \sin\theta d\theta + \int_B f_2 \sin\theta d\theta + \int_C f_3 \sin\theta d\theta + \int_D f_4 \sin\theta d\theta\right] \quad (5)$$

where A, B, C and D denote integral ranges of each voltage function as shown in Fig. 4.

Since $F(\alpha_r)$ represents the peak value of the fundamental component, it can be calculated from the definition of the modulation index.

$$F(\alpha_r) = \frac{2}{\pi} \cdot V_{dc} \cdot MI \quad (6)$$

Thus, a relationship between the MI and the reference angle which gives a linearity of the output voltage is determined. The equation of the piecewise-linear reference angle (α_r) as a function of the MI is shown from (7) to (9).

$$\alpha_r = -30.23 \times MI + 27.04 \qquad (0.9068 \le MI \le 0.9095) \quad (7)$$

$$\alpha_r = -8.580 \times MI + 8.230 \qquad (0.9095 \le MI \le 0.9485) \quad (8)$$

$$\alpha_r = -26.43 \times MI + 25.15 \qquad (0.9485 \le MI \le 0.9517) \quad (9)$$

As established in Fig. 4, the upper limit in the over-modulation region I is $\alpha_r = 0°$. MI at this condition is 0.952, which is driven in (5) and (6). Therefore when the MI is higher than 0.952, another over-modulation algorithm is necessary.

2) Over-modulation region II $(0.952 \le MI \le 1)$

Under such conditions, output voltages higher than MI=0.952 can not be generated since there exists no more surplus area to compensate for the voltage loss even though the modulation index is increased above that point. As a result, over the compensation limit by using the technique in the over-modulation region I, V_r^* is held during holding angle α_h for the compensation of voltage loss when V^* is rotating according to time. This is called over-modulation region II. To control the holding angle of the time interval, the active switching state remains at the vertices which uniquely control the fundamental voltage. A basic concept of the over-modulation region II is similar to (5) and (6). Regions of V_r^* present four kinds of equations per π/2 as the angle of reference voltage vector, α_h, as shown from (10) to (13). The value of the fundamental component of V_r^* is directly proportional to MI. Figure 6 shows the trajectory of the reference voltage vector and phase voltage waveform in the overmodulation region II.

$$f_1 = \frac{V_{dc}}{\sqrt{3}} \tan\alpha_p \qquad 0 \le \theta \le \left(\frac{\pi}{6} - \alpha_h\right) \quad (10)$$

$$f_2 = \frac{V_{dc}}{3} \qquad \left(\frac{\pi}{6} - \alpha_h\right) \le \theta \le \left(\frac{\pi}{6} + \alpha_h\right) \quad (11)$$

$$f_3 = \frac{V_{dc}}{\sqrt{3}\cos\left(\frac{\pi}{3} - \alpha_p'\right)} \sin\alpha_p' \qquad \left(\frac{\pi}{6} + \alpha_h\right) \le \theta \le \left(\frac{\pi}{2} - \alpha_h\right) \quad (12)$$

$$f_4 = \frac{2V_{dc}}{3} \qquad \left(\frac{\pi}{2} - \alpha_h\right) \le \theta \le \frac{\pi}{2} \quad (13)$$

where

$$\alpha_p = \frac{\pi}{\pi - 6\alpha_h}\theta \quad \text{and} \quad \alpha_p' = \left(1 - \frac{6}{\pi}\alpha_h\right)\theta' \qquad \left(\theta' = \theta - \frac{\pi}{6}\right) \quad (14)$$

In (14), α_p and α_p' are phase angles of the actual voltage reference vector rotating as shown in Fig. 7, which is simply driven from the proportional relationship for angular displacements of these two vectors as

$$\theta : \alpha_p = \frac{\pi}{6} : \left(\frac{\pi}{6} - \alpha_h\right). \quad (15)$$

Thereafter, the actual voltage reference vector is held at the vertex while the fundamental one is continuously rotating from $\theta = ((\pi/6) - \alpha_h)$ to $\pi/6$. Also the piecewise-linear holding angles (α_h) as a function of the MI are shown as from (16) to (18).

$$\alpha_h = 6.40 \times MI - 6.09 \qquad (0.9517 \le MI \le 0.9800) \quad (16)$$

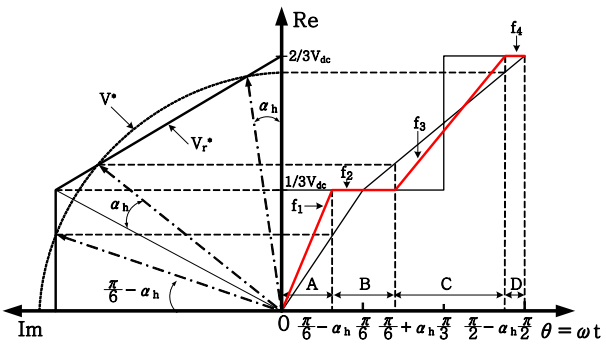

Fig. 6. Trajectory of reference voltage vector and phase voltage waveform in over-modulation region I I.

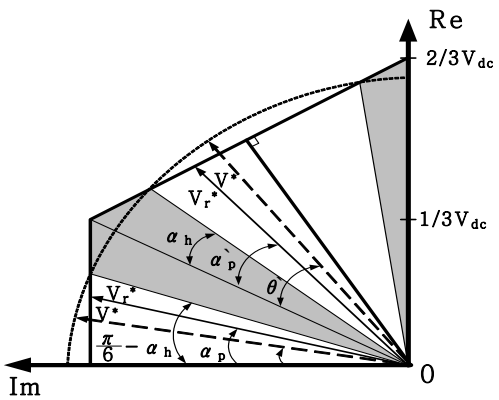

Fig. 7. Angular displacement of reference and actual voltage Vector.

$$\alpha_h = 11.75 \times MI - 11.34 \qquad (0.9800 \le MI \le 0.9975) \qquad (17)$$

$$\alpha_h = 48.96 \times MI - 48.43 \qquad (0.9975 \le MI \le 1.0000) \qquad (18)$$

3. Simulation Results

The validity of the proposed algorithm is verified through the simulation for the three-level inverter with induction motor.

The indirect vector control method utilizes the motor velocity feedback and a feed-forward slip reference to provide the instantaneous torque control. A schematic diagram of indirect vector control of the induction motor with PI controllers is shown in Fig. 8. The feed-forward EMF block in current controlled VSI is required to produce the appropriated stator voltage, and the flux reference block

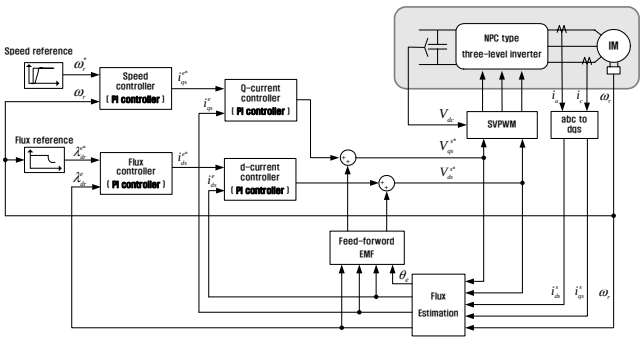

Fig. 8. Schematic diagram of indirect vector control of induction motor.

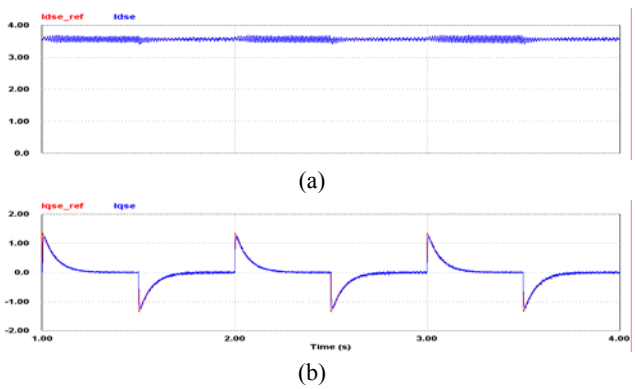

Fig. 9. Response of current controllers under repeated motor speed change between 500rpm and 1000rpm for; (a) flux component, (b) torque component.

is included to increase the response speed beyond the nominal speed [13]-[15].

The simulation results of indirect vector control are shown in Figs. 9 and 10. Figure 9 shows the response of the current controller for flux component current and torque component current when the reference motor speed changes from 500rpm to 1000rpm frequently. As the speed reference value changes, the torque component current is regulated to generate the positive and negative value in acceleration and deceleration regions. The flux component current is also well regulated to follow the reference value without any change under the speed change condition. Figure 10 shows the magnitude and phase of reference voltage vector in stationary reference frame during the transient state of motor speed change. They change in linear relation to the speed change.

The simulation results of operation for the three-level

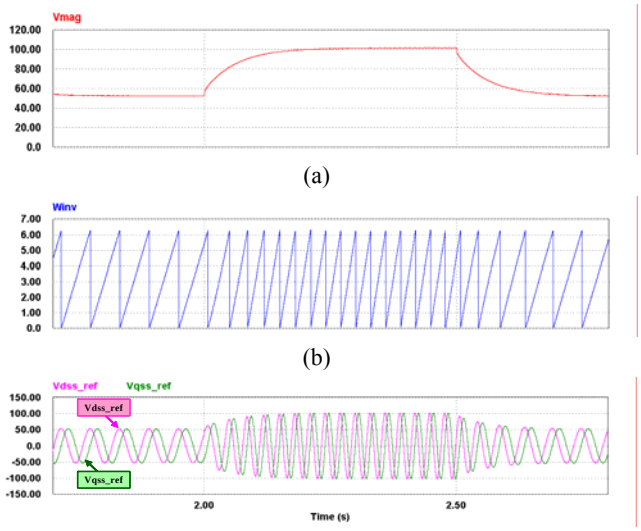

Fig. 10. Voltage reference of NPC type three-level inverter; (a) magnitude of voltage reference in stationary frame, (b) angle of that, (c) dq components of voltage vector in stationary frame.

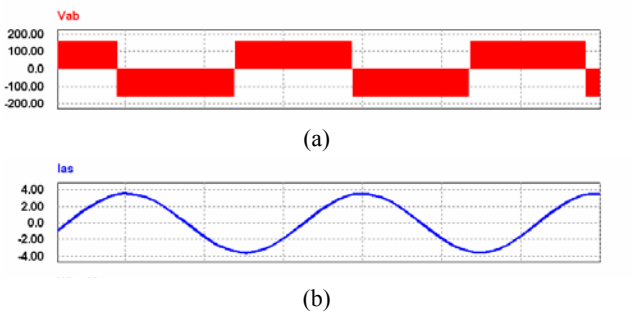

Fig. 11. Simulation results at MI=0.369; (a) line to line voltage and (b) phase current.

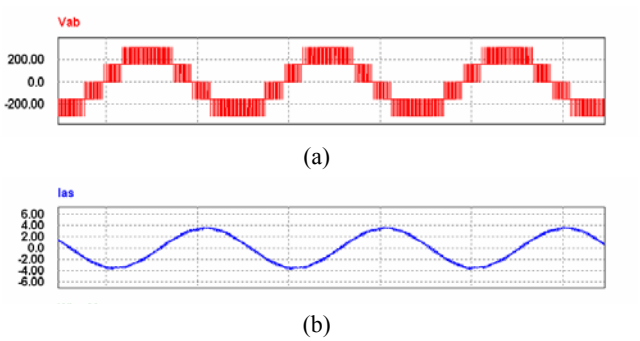

Fig. 12. Simulation results at MI=0.767; (a) line to line voltage and (b) phase current.

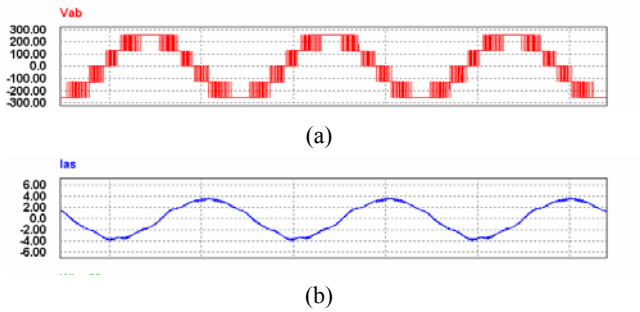

Fig. 13. Simulation results at MI=0.936; (a) line to line voltage and (b) phase current.

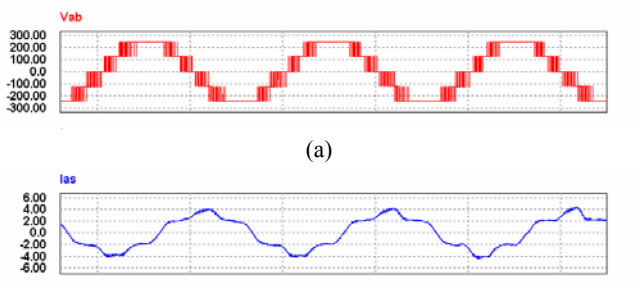

Fig. 14. Simulation results at MI=0.974; (a) line to line voltage and (b) phase current.

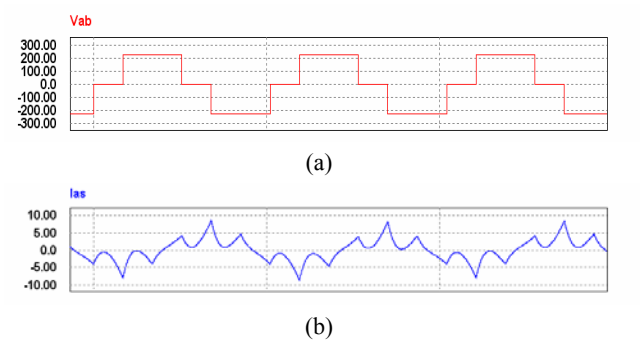

Fig. 15. Simulation results at MI=1; (a) line to line voltage and (b) phase current.

inverter following each region are shown in from Fig. 11 to 15. These figures show the results of phase current and line-to-line voltage waveforms when MI is 0.369 (Fig. 11) in the linear region mode I, 0.767 (Fig. 12) in the linear region mode II, 0.936 (Fig. 13) in the over-modulation region I, and 0.974 (Fig. 14) and 1 (Fig. 15) in the over-modulation region II, respectively. In Fig. 11, the line-to-line voltage has the same characteristic as that of two-level inverter. In Fig. 12, the line-to-line voltage has 5

steps so the harmonic level is much less than that of the two-level inverter. In Fig. 13, as an example of overmodulation region I, one of two sectors of 2 and 4 is selected as a small sector for the large sector A. As shown in Fig. 15, it is operated as a six-step mode at MI=1, and then the holding angle of each small sector is $\pi/6$.

Table 4 Induction motor rating and parameters

Rating		Parameter specification	
Power	0.75[kW]	stator resistance, R_s	3.5 [Ω]
Pole number	4	rotor resistance, R_r	2.448 [Ω]
Y/Δ voltage	380/220[V]	Stator leakage inductance, L_s	133.3 [mH]
Y/Δ current	2.2/3.8[A]	rotor leakage inductance, L_r	133.3 [mH]
speed	1680[rpm]	mutual inductance, L_m	129.0 [mH]
frequency	60[Hz]	Inertia of wheel, J_e	0.0023[Kgm^2]

4. Experimental Results

A digital signal processor (DSP) TMS320VC33 is used as a control board. The rate and parameter of the induction motor used for experiments are shown at Table IV and Table V. Figure 16 shows the front view of the experimental system. For the pilot load of traction drives, a large flywheel system driving with four induction motors is used in the experiment.

The experimental results are shown in Fig. 17 to 18 at the same condition used in simulation. Figure 17 shows the response of current controller with the current waveforms of flux component and torque component when the reference motor speed changes from 500rpm to 1000rpm or vice versa. As the speed reference value changes, the flux current components are well regulated to follow the reference value. Also, the torque current component is regulated to generate the positive and negative value as the change of acceleration and deceleration region.

Figure 18 shows magnitude and angle of voltage reference vector when the reference of motor speed changes. Also it shows flux component and torque component of voltage reference vector. The flux component and torque component of the voltage reference vector in the stationary frame is orthogonal for $\pi/2$ always.

Fig. 16. Picture of experiment system.

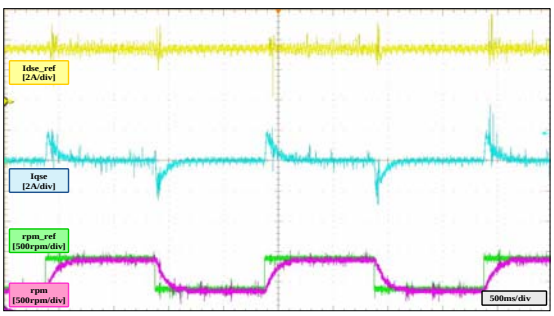

Fig. 17. Experimental results; (top) flux component, (middle) torque current component, (bottom) speed.

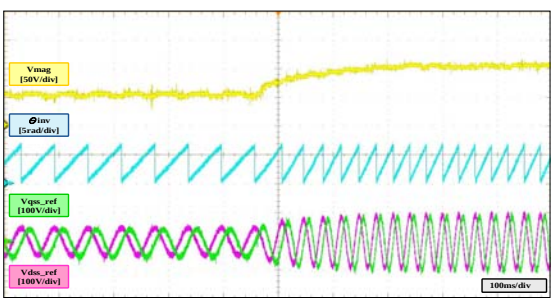

Fig. 18. Experimental results; (top) voltage magnitude, (middle) phase angle, (bottom) dq components of voltage vector in stationary frame.

The experimental results of operation for three-level inverter following each region are shown in Fig. 19 to 23. Conditions of each operation region are given in Table 5. The line to line voltages are measured by a differential probe (100:1) and the phase currents are done by current probe (1A:20mV).

Figure 19 shows the results of phase current and line-to-line voltage when MI is 0.369 in the linear region mode I. The line-to-line voltage has the same characteristic as that of two-level inverter and small sector is covered only

Table 5 Operation of three-level inverter following modulation index

ω_{rpm}	V_{dc}	V_{mag}	MI	Region
500	311	72	0.369	Liner region Ⅰ
1500	311	151.93	0.767	Liner region Ⅱ
1500	255	151.93	0.936	Over-modulation region Ⅰ
1500	245	151.93	0.974	Over-modulation region Ⅱ
1500	228	151.93	1.0	Six-step operation

by 1 for large sector. Fig. 20 shows the results of phase current and line-to-line voltage when MI is 0.767 in the linear region mode II. The line-to-line voltage has 5 steps so the harmonic level is much less than that of two-level inverter. Fig. 21 shows the results of phase current and line-to-line voltage when MI is 0.936 in the over-modulation region I. Figures 22 and 23 show the results of phase current and line-to-line voltage when MI is 0.974 and 1 in the over-modulation region II. Holding angle α_h is increased when the modulation index is increased at this region. The region of MI=1 is an operated six-step mode. And holding angle of each small sector is $\pi/6$.

5. Conclusion

In this paper, a PI controller for indirect vector control of an induction motor and SVPWM technique for an NPC type 3-level inverter from linear region to six-step operation was proposed. With this proposed over-modulation strategy, the output voltage of the three-level inverter can be controlled in an extended range from MI=0.907 to the unit. The proposed algorithm was verified through simulation and experimental results with the phase current and line-to-line voltage waveforms as the typical values of the modulation index from the linear region to the over-modulation region. Also, it was simulated with the three-level inverter fed induction motor drives and well verified with regulation performance under the dc-link voltage change and speed change conditions.

Acknowledgment

This research was supported in part by grant R01-2006-000-10811-0 from the Basic Research Program of the Korea Science & Engineering Foundation and supported by the Ministry of Education, Science Technology (MEST) and Korea Industrial Technology Foundation (KOTEF) through the Human Resource Training Project for Regional Innovation.

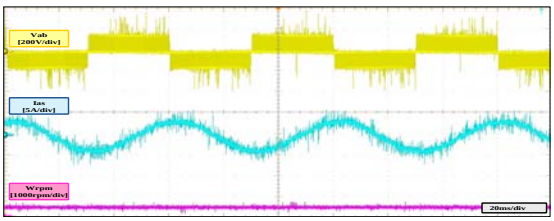

Fig. 19. Experimental results at MI=0.369; (top) line to line voltage, (middle) phase current, (bottom) speed.

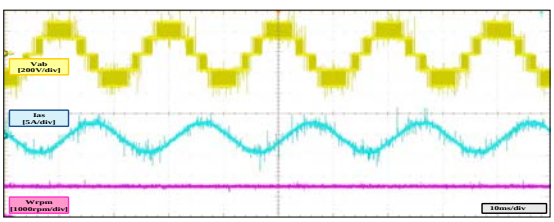

Fig. 20. Experimental results at MI=0.767; (top) line to line voltage, (middle) phase current, (bottom) speed.

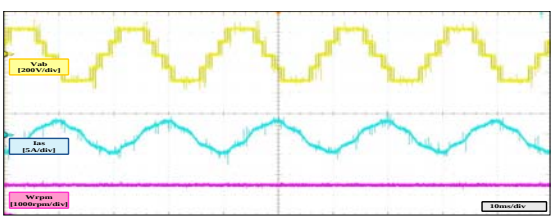

Fig. 21. Experimental results at MI=0.936; (top) line to line voltage, (middle) phase current, (bottom) speed.

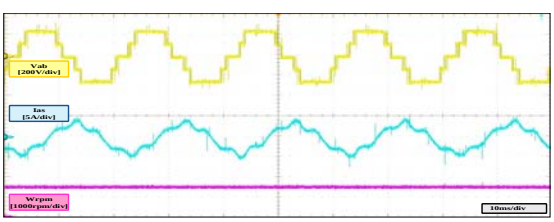

Fig. 22. Experimental results at MI=0.974; (top) line to line voltage, (middle) phase current, (bottom) speed.

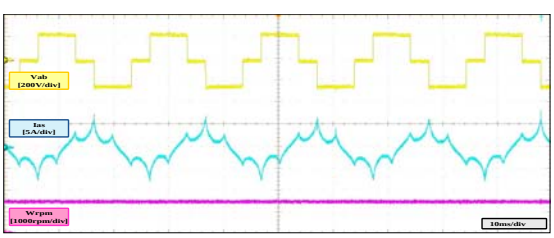

Fig. 23. Experimental results at MI=1; (top) line to line voltage, (middle) phase current, (bottom) speed.

References

[1] J. Holtz, W. Lotzkat, and A. M. Khambadkone, "On continuous control of PWM inverters in the overmodulation range including the six-step mode," *IEEE Trans. Power Electron*., Vol. 8, No. 4, pp. 546-553, 1993.

[2] D. Lee and G. Lee, "A Novel Overmodulation technique for space-vector PWM inverters," *IEEE Trans. Power Electron*., Vol. 13, No. 6, pp. 1144-1151, 1998.

[3] A. Nabae, I. Takahashi, and H. Akagi, "A new neutral point clamped PWM inverter," *IEEE Trans. Ind. Appl*., IA-17,(5), pp. 518-523, 1981.

[4] A. Horie, S. Saito, S. Ito, T. Takasaki, and H. Ozawa "Development of a three-level converter-inverter system with IGBT's for AC electric cars," *in Conf. Rec. IEE Japan IAS Annu. Meet. Rec.*, pp.75-78, 1995.

[5] E. Akagawa, S. Kawamoto, S. Tamai, H. Okayama, and T. Uemura, "Three-level PWM converter-inverter system for next-generation Shinkansen," *in Conf. Rec. IEE Japan IAS Annu. Meet. Rec.*, pp.81-82, 1995.

[6] C. Ma, T. Kim, D. Kang, and D. Hyun, "A simple control strategy for balancing the DC-link voltage of neutral-point-clamped inverter at low modulation index," *Journal of Power Electronics*, Vol. 3, No. 4, pp. 205-214, 2003.

[7] W. Oh, S. Han, S. Choi, G. Moon, "A three phase three-level PWM switched voltage source inverter with zero neutral point potentional," *Journal of Power Electronics*, Vol. 5, No. 3, pp. 224-232, 2005.

[8] S. K. Mondal, J. O. P. Pinto, and B. K. Bose, "A neural-network-based space-vector PWM controller for a three-level voltage-fed inverter induction motor drive," *IEEE Trans. Ind. Appl*., Vol. 38, No. 3, pp. 660-669, 2002.

[9] S. K. Modal, B. K. Bose, V. Oleschuk, and J. O. P. Pinto, "Space vector pulse width modulation of three-level inverter extending operation into overmodulation region", *in Conf. Rec. IEEE PESC'02*, Vol. 2, pp. 497-502, 2002.

[10] S. Jin, Y. Zhong, and W. Cheng, "Novel SVPWM overmodulation scheme and its application in three-level inverter," *in Conf. Rec. IEEE PESC'06*, pp.1-6, 2006.

[11] S. Venugopal and G. Narayanan, "An overmodulation scheme for vector controlled induction motor drives," *in Conf. Rec. IEEE PEDS'06*, pp. 1-6, 2006.

[12] J. Lee, J. Choi, and Y. Nishida, "Overmodulation strategy of NPC type 3-level inverter for traction drives," *in Conf. Rec. ICPE'07*, pp. 137-142, 2007.

[13] Rowan, T.M., Kerkman, R.J. and Leggate, D, "A simple on-line adaption for indirect field orientation of an induction machine," *IEEE Trans. Industry Applications*. Vol.27, Issue 4, pp.720-727, 1991.

[14] Bimal K. Bose, *Modern Power Electronics and AC Drivers*, pp.368-387, Prentice-Hall, Inc., 2002.

[15] D. Grahame Holmes and Thomas A. Lipo, *Pulse width modulation for power converters*, pp. 349-382, A John wiley & Sons, Inc., 2003.

Kyoung-Min Kwon received his B.S. degree in Electrical Engineering from Chungbuk National University in Cheongju, Korea in 2006, where he is currently working toward his M.S. degree. He was a Junior Research Engineer at the Controller R&D Center in Woojin Industrial System from 2006 to 2008. His research interests are in ac motor drives with power converter/inverter systems, wind power generation systems and energy storage systems.

Jae-Moon Lee received his B.S. and M.S. degrees in Electrical Engineering from Chungbuk National University in Cheongju, Korea in 2006 and 2008, respectively. He has been an Associate Research Engineer at the Drive Research Team Automation R&D Center in LS Industrial Systems since 2008. His research interests are in AC machine drives, Power Electronics and Power systems.

Jin-Mok Lee received his B.S. and M.S. degrees in Electrical Engineering from Chungbuk National University in Cheongju, Korea in 2002 and 2004, respectively, where he is currently working toward his PhD. His research interests are in power quality analysis and controller design of power converters and inverter systems.

Jaeho Choi received his B.S., M.S., and Ph. D in Electrical Engineering from Seoul National University, Seoul, Korea in 1979, 1981, and 1989, respectively. From 1981 to 1983, he was with Jungkyoung Technical College, Daejeon, Korea, as a Full-time Lecturer. Since 1983, he has been with the School of Electrical and Computer Engineering, Chungbuk National University in Cheongju, Korea, where he is currently a professor. In 1993, 1998 and 2003, he was a visiting professor at the University of Toronto, Canada, each for one year and he was a Danfoss Visiting Professor at Aalborg University in Denmark in 2000. His research areas include power electronics, power quality problems and solutions, energy storage systems, and renewable energy and microgrid systems. He is an active member of KIEE, KIPE, and IEEE, and currently the Editor-in-Chief of JPE.